Assessment of reduced-order models in analysis of Floquet modes in an infinite periodic elastic layer

Hvatov, Alexander; Sorokin, Sergey

Published in:
Journal of Sound and Vibration

DOI (link to publication from Publisher):
10.1016/j.jsv.2018.10.034

Publication date:
2019

Document Version
Accepted author manuscript, peer reviewed version

Accepted Manuscript

Assessment of reduced-order models in analysis of Floquet modes in an infinite periodic elastic layer

Alexander Hvatov, Sergey Sorokin

PII: S0022-460X(18)30707-7

DOI: https://doi.org/10.1016/j.jsv.2018.10.034

Reference: YJSVI 14450

To appear in: *Journal of Sound and Vibration*

Received Date: 28 August 2018

Revised Date: 16 October 2018

Accepted Date: 18 October 2018

Please cite this article as: A. Hvatov, S. Sorokin, Assessment of reduced-order models in analysis of Floquet modes in an infinite periodic elastic layer, *Journal of Sound and Vibration* (2018), doi: https://doi.org/10.1016/j.jsv.2018.10.034.

Assessment of reduced-order models in analysis of Floquet modes in an infinite periodic elastic layer

Alexander Hvatov

Department of Physics, State Marine Technical University of St. Petersburg, Lotsmanskaya 3, 190008, St. Petersburg, Russia

eScience Research Institute, ITMO University, Kronversky pr. 49, 197101, St. Petersburg, Russia

Sergey Sorokin

Department of Materials and Production, Aalborg University, Fibigerstrade 16, DK9220, Aalborg, Denmark

Abstract

A hierarchy of reduced-order models of wave propagation in a periodic elastic layer is used to study the periodicity-induced stop-band effects. At each approximation level, the eigenfrequency problem for a unit symmetric periodicity cell with appropriate boundary conditions is shown to be equivalent to the problem of identification of frequencies separating pass- and stop-bands. Factorization of eigenfrequency equations and of equations defining positions of pass- and stop-bands for individual Floquet modes is demonstrated. The difference between accuracy levels of reduced order models for homogeneous and periodic layers is highlighted and explained.

Keywords: wave propagation, periodic elastic layer, reduced-order models, Floquet theory, pass- and stop-bands, eigenfrequency spectra

1. Introduction

Starting with the pioneering work of Brillouin [1] , wave propagation in periodic media has been studied in numerous publications referred to various realms of physics (acoustics, optics, electromagnetics, elastodynamics, geophysics, etc.). In structural dynamics, seminal papers by Mead [2, 3, 4] stipulated research in periodicity-induced vibro-isolation for beam-plate- and shell-type structures. In the most of engineering applications, the vibro-isolation analysis is typically confined to the low-frequency region, where elementary theories, or models (Bernoulli-Euler, Timoshenko) are valid. However, as is well known stop bands emerge in a periodic structure, when a frequency become sufficiently high. Then high-order waves (ignored by the elementary theories) can transform from evanescent to propagating

Email addresses: matematik@student.su, corresponding author (Alexander Hvatov), svs@mp.aau.dk (Sergey Sorokin)

ones and, therefore, make a periodic structure more 'transparent' for the energy flow. Thus, stop band predictions based on the use of elementary models become erroneously optimistic above cut-off frequencies of its constituents. In view of the growing interest in the periodicity-induced vibration isolation of large-scale structures (e.g., components of wind turbines), which have fairly low cut-off frequencies of high-order waves, the modelling of periodicity effects beyond the applicability limits of elementary theories acquires practical relevance. In what follows, we use the canonical Rayleigh-Lamb problem as a convenient case-study, which highlights phenomena, existing in a broad range of multi-modal periodic waveguides.

Of course, the high-frequency wave propagation in periodic elastic waveguides, in particular, in a straight elastic periodic layer of a constant thickness is a classical subject thoroughly treated in many research papers with [5, 6, 7] being just a few examples. In these references, the Floquet-Bloch waves are described in the framework of exact Rayleigh-Lamb formulation, and the existence of high-frequency stop-bands is documented. The efficient analytical and numerical methods have been used in [7] for solving the problem in its original 2D formulation, and the results reported there are valid for virtually any frequency range. However, some physically meaningful issues have not yet been explored in full details, especially at moderately high frequencies. The reason is that the approximate solutions of such a challenging problem contain details, which inevitably mask the essential features of periodicity effects. We are of opinion that the reduced order modelling is the preferred option to highlight and explain these features. Therefore, we are interested in the situations, when the elementary Bernoulli-Euler model breaks down, but the full Rayleigh-Lamb model is yet not needed to describe wave propagation in constituents of a periodic layer.

In references [8, 9], a hierarchy of reduced order models has been formulated and validated for both symmetric and skew-symmetric waves in a homogeneous layer. These models accurately capture a prescribed number of branches of the dispersion diagram and, therefore, may be used to identify the location of pass- and stop-bands in the frequency range of our interest and to study the essential periodicity effects in multi-modal waveguides, not yet fully explored in the literature.

In particular, as has been shown in [10] for several examples, the eigenfrequency problem for symmetric periodicity cells with certain boundary conditions is equivalent to the problem of finding frequencies separating stop- and pass-bands in an infinite structure composed of these cells. This result needs a closer inspection in the cases, when constituents of a periodic structure support several waves. The same holds true regarding analysis of composition of Floquet waves in a multi-modal waveguide.

Since the phenomena observed in the cases of symmetric and skew-symmetric waves are virtually the same [9], we consider only the former ones. To capture the tendencies in performance of periodic structures at high frequencies, it is sufficient to consider three models of progressive complexity, that is a single mode Bernoulli model,a three-mode and a five-mode ones. Although these models are fully explained in [8, 9], we briefly introduce them in Sec.2. In Sec.3 results of analysis of stop- and pass-band locations are presented. The eigenfrequency analysis is performed in Sec.4. Comparison of the three models is done in Sec.5, and the main novel results are summarized in Conclusions.

2. The hierarchy of reduced-order models of a straight elastic layer

We consider time harmonic free waves in a periodic elastic layer schematically illustrated in Fig.1 and employ the canonical formulation of Rayleigh-Lamb problem (i.e., a layer with no damping in plane strain).

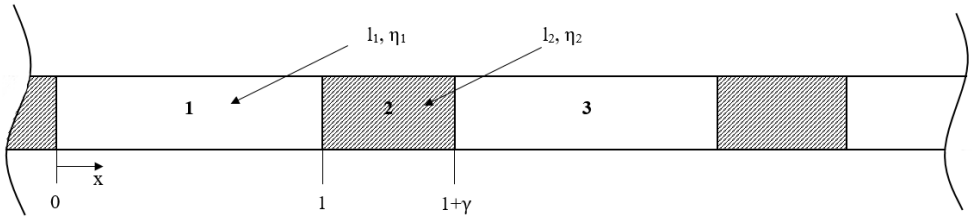

Figure 1: Periodic elastic layer

Each segment is characterized by its own dilatation wave speed $c_1^{(i)}$, shear wave speed $c_2^{(i)}$, and length l_i. The thickness is assumed to be the same, $h_1 = h_2 = h$. We introduce the parameter $\eta_i = \frac{c_1^{(i)}}{c_2^{(i)}}$ for each segment and assume that the shear wave speed is changing insignificantly, so that $c_2^{(1)} = c_2^{(2)} = c_2$. The dimensionless parameters are

$$\sigma = \frac{\eta_2}{\eta_1}\ \gamma = \frac{l_2}{l_1}\ \lambda = \frac{h_1}{l_1} \tag{1}$$

If it is not stated otherwise, following numerical values of non-dimensional parameters are used

$$\lambda = 0.3\ ; \sigma = 0.7\ ; \gamma = 10 \tag{2}$$

The reported hereafter results are fully representative and the parametric studies, which have been conducted, demonstrate just quantitative changes in performance of a periodic layer.

As discussed in the Introduction, propagation of symmetric wave in each block is described by means of three reduced-order theories, which are derived and thoroughly explained in [8, 9]. For consistency, in Appendix A, we reproduce the governing equations without derivation details, which are readily available in the above-mentioned papers.

It is expedient to introduce following vector definitions, which relate the components of decomposition on Legendre polynomials to the physical variables.

$$\begin{array}{ll} \mathbf{u}_i(x) = \{U_0(x), U_2(x), U_4(x)\}; & \sigma_{xy}^{(i)}(x) = \{F_1(x), F_3(x)\}; \\ \mathbf{v}_i(x) = \{V_1(x), V_3(x)\}; & \sigma_{xx}^{(i)}(x) = \{F_0(x), F_2(x), F_4(x)\}; \end{array} \tag{3}$$

In Eq.(3) vector $\mathbf{u}_i(x)$ contains the Legendre polynomial decomposition modes of axial displacement of i-th segment, $\mathbf{v}_i(x)$ is the decomposition modes of flexural displacement.

Vector $\sigma_{jk}^{(i)}(x)$ contains stress tensor decomposition modes $F_j^{(i)}$. More detailed description of Legendre polynomial decomposition modes and dispersion relation are contained in Appendix A. In Eq.(3) decomposition modes, specific for 1-mode have index 0, for 3-mode theory have indices $0, 1, 2$, 5-mode theory is fully covered by Eq.(3).

With dependence of all state variables taken as $\exp(ikx - i\omega t)$ one can obtain dispersion relation $k(\Omega)$, where $\Omega = \frac{\omega h_1}{c_1^{(1)}}$. Waveguide properties of a n-mode approximation are clearly seen from comparative dispersion diagram plotted in Fig.2 for white segments (see Fig.1):

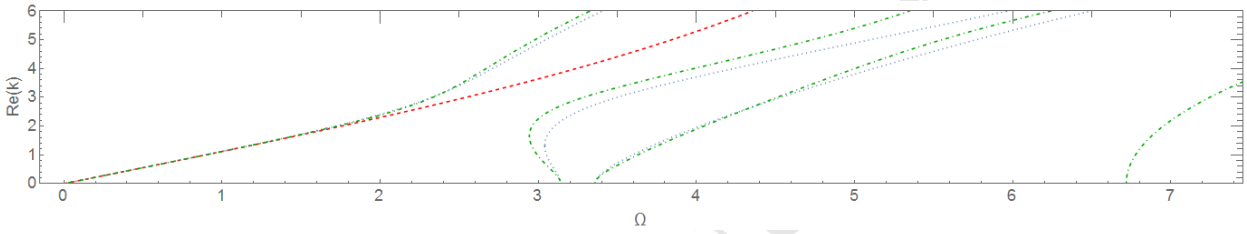

Figure 2: 1,3,5-modes theory dispersion diagram (dashed, dotted, dot-dashed)

In the frequency-wavenumber window presented in Fig.2, exact dispersion curves are overlapped by their counterparts predicted by 5-mode theory.

A periodic layer, shown in Fig.1, contains also grey segments, which have dispersion diagram and cut-off frequencies shifted as compared with their counterparts shown in Fig.2. In Fig.3, solid/dashed lines present dispersion curves for white/grey segments obtained in the framework of the 5-mode model in the somewhat broader frequency range, than in Fig.2. The scaling is done with the reference to white segments, i.e., $\Omega = \frac{\omega h_1}{c_1^{(1)}}$

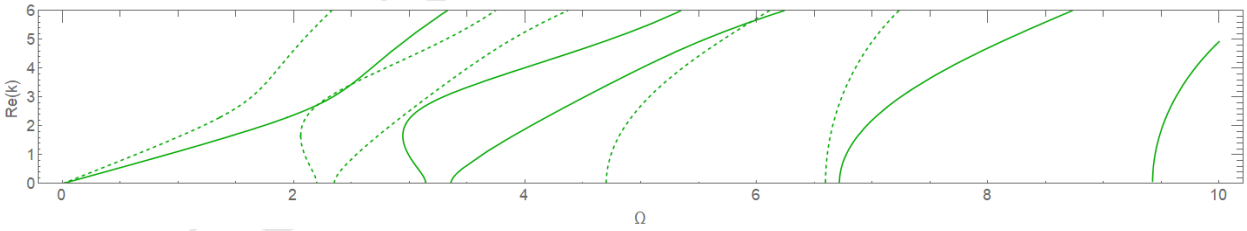

Figure 3: 5-modes theory dispersion diagram (solid – white segments, dashed – grey segments)

As seen from Fig.3, there is a substantial difference between cut-off frequencies of constituents of a periodic layer. As will be seen, this feature of the bi-component periodic layer affects both the formation of stop-bands in an infinite structure and the composition of eigenfrequency spectra of periodicity cells.

3. An infinite periodic layer

Within this Section, the hierarchy of reduced-order models is used in frame of Floquet theory. All results reported hereafter are obtained by means of boundary equations/Green's matrix method. In the simple cases of Bernoulli-Euler and 3-mode models, the conventional

transfer matrix method has also been applied and exactly the same results obtained. However, the transfer matrix method is inherently unstable due to the presence of exponentially growing/decaying waves besides the propagating ones [11]. These waves must be taken into account in the 3-mode and 5-mode models. Therefore, to ensure numerical stability for any set of parameters, the Green's matrix method is used as described in [8, Section 6] and [9, Sections 3-4].

The applicability of the reduced-order models, as well as of the Green's matrix/boundary integral equations method has been validated for the homogeneous waveguides in the references [8, 9]. Likewise, application of the Floquet theory in the problem in hand is fairly straightforward. Therefore, we leave further verification, i.e., by means of finite element method, out of the scope of this paper.

3.1. Floquet analysis

We consider three consequent segments indicated in Fig.1. Interfacial conditions have the form

$$\begin{array}{rr} \mathbf{u}_1(1) = \mathbf{u}_2(1); & \mathbf{u}_2(1+\gamma) = \mathbf{u}_3(1+\gamma); \\ \mathbf{v}_1(1) = \mathbf{v}_2(1); & \mathbf{v}_2(1+\gamma) = \mathbf{v}_3(1+\gamma); \\ \sigma_{xx}^{(1)}(1) = \sigma_{xx}^{(2)}(1); & \sigma_{xx}^{(2)}(1+\gamma) = \sigma_{xx}^{(3)}(1+\gamma); \\ \sigma_{xy}^{(1)}(1) = \sigma_{xy}^{(2)}(1); & \sigma_{xy}^{(2)}(1+\gamma) = \sigma_{xy}^{(3)}(1+\gamma); \end{array} \tag{4}$$

The periodicity conditions are:

$$\begin{array}{r} \mathbf{u}_1(0) = \Lambda \mathbf{u}_3(1+\gamma); \\ \mathbf{v}_1(0) = \Lambda \mathbf{u}_3(1+\gamma); \\ \sigma_{xx}^{(1)}(0) = \Lambda \sigma_{xx}^{(3)}(1+\gamma); \\ \sigma_{xy}^{(1)}(0) = \Lambda \sigma_{xy}^{(3)}(1+\gamma); \end{array} \tag{5}$$

Here Λ is the propagation constant, introduced in Floquet theorem. It is linked to Bloch propagation constant K_B by the relation $\Lambda = \exp(iK_B)$.

Equations Eqs.(4-5) involve vectors of Legendre polynomial projection modes Eq.(3), so that in the component form the systems of algebraic equations are of different length for Bernoulli-Euler,3 -mode and 5-mode theories. These equations are supplemented with boundary equations for each segment (see technical details in [9, Secton 4]). Then a homogeneous system of linear algebraic equations of order 12, 36 and 60 with respect to the modal amplitudes is assembled. Equating its determinant to zero yields polynomial equation in Λ of the second, sixth and tenth order for 1-, 3- and 5-modes theory respectively.

Let $m = 1, 3, 5$ be the amount of modes accounted for in a reduced-order theory. It can be shown directly that the determinants have following common form

$$D^{(m)}(\Lambda, \Omega) = \prod_{j=1}^{m} (\Lambda^2 + a_{m,j}(\Omega)\Lambda + 1) = \prod_{j=1}^{m} D_j^{(m)}(\Lambda, \Omega) \tag{6}$$

In the elementary Bernoulli theory (i.e., then $m = 1$), Eq.(6) reduces to a quadratic one, because at this approximation level the waveguide supports a single Floquet mode, which

may be either propagating (pass-band) or evanescent (stop-bands). The Floquet mode in a pass-band is a composite wave. In a pass-band it is sinusoidal only piece-wise (i.e., within each segment), and these sinusoidal fragments are defined by different wavenumbers. Naturally, the pass-band Floquet mode specifies a pair of identical composite waves travelling in opposite directions. The Floquet mode in a stop-band consists of the same ingredients, but their amplitude decays from the left to the right in one composite wave and in the opposite direction in the other [10].

The difference between Floquet modes in stop- and pass-bands is characterized by the propagation constant Λ. Zones, where $\mathrm{abs}(\Lambda) = 1$ are pass-bands, and zones, where $\mathrm{abs}(\Lambda) \neq 1$ are stop-bands. The Vieta's formula for the roots of the quadratic polynomial: $\Lambda^{(1)} * \Lambda^{(2)} = 1$ (i.e. the product of roots is equal to the free term) proves that the characteristics of waves travelling/decaying in the opposite directions are identical. These zones are shown in Fig.4, lower part. In what follows we illustrate our results as shown in the upper part of Fig.4 with not colored spaces designating positions of stop bands for an individual Floquet mode.

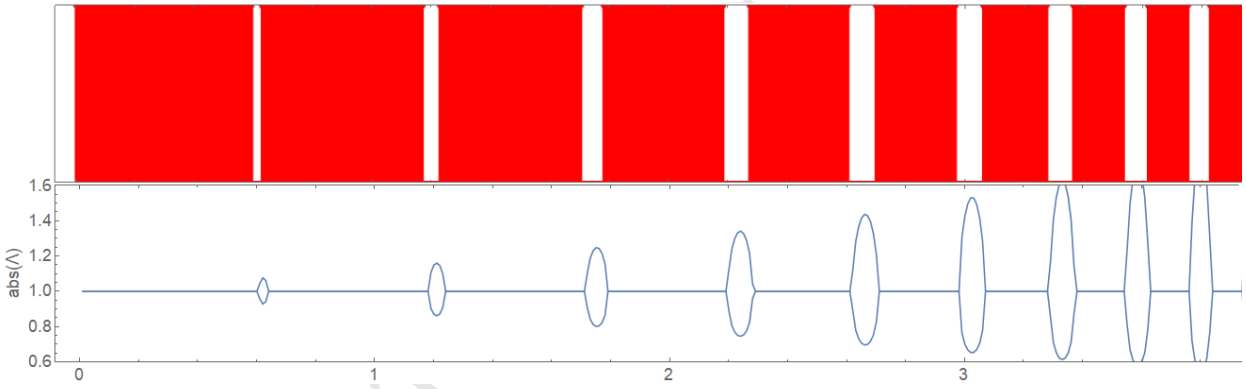

Figure 4: Zeroes of determinant from relation $D^{(1)}(\Lambda, \Omega) = 0$ (lower), 1-mode approximation theory and stop-band scheme (upper): color – pass-bands, white – stop-bands

Direct computation show that m pairs of propagation constants, and, therefore, m Floquet modes exist in the waveguide modelled by the m-mode theories . For each mode, the symmetry property ${\Lambda_1}^{(1)} * {\Lambda_1}^{(2)} = ... = {\Lambda_m}^{(1)} * {\Lambda_m}^{(2)} = 1$ is held regardless whether the constants are found for a pass- or a stop-band. This gives implicit form of decomposition Eq.(6)

$$\begin{aligned} D^{(m)}(\Lambda, \Omega) = \prod_{j=1}^{m} (\Lambda - \Lambda_j^{(1)})(\Lambda - \Lambda_j^{(2)}) = \prod_{j=1}^{m} (\Lambda^2 - (\Lambda_j^{(1)} + \Lambda_j^{(2)}) + \Lambda_j^{(1)}\Lambda_j^{(2)}) \\ = \prod_{j=1}^{m} (\Lambda^2 - (\Lambda_j^{(1)} + \Lambda_j^{(2)}) + 1) \end{aligned} \tag{7}$$

Moreover, Eq.(7) gives explicit form for $a_{1,j}(\Omega)$ and for $D_j^{(m)}(\Lambda, \Omega)$ in Eq.(6) as

$$a_{m,k}(\Omega) = -(\Lambda_k^{(1)} + \Lambda_k^{(2)}) \tag{8}$$

A partial Floquet binomial $D_j^{(m)}(\Lambda, \Omega)$ determines waveguide properties of the individual Floquet mode. Following [10], one can show that stop-band boundaries of $i-th$ mode are defined by discriminant of the binomial $D_j^{(m)}(\Lambda, \Omega)$ with condition

$$\mathrm{discr}(D_j^{(m)}) = 0, i = 1, ..., m \tag{9}$$

The discriminant of polynomial equation is designated as discr . Since $D_j^{(m)}(\Lambda, \Omega)$ have no common roots, following equation holds true

$$\mathrm{discr}(D^{(m)}) = \prod_{j=1}^{m} \mathrm{discr}(D_j^{(m)}(\Lambda, \Omega)) \tag{10}$$

Using Eqs.(6-8) we can illustrate stop- and pass-band picture for parameter set Eq.(2) as shown in Fig.5

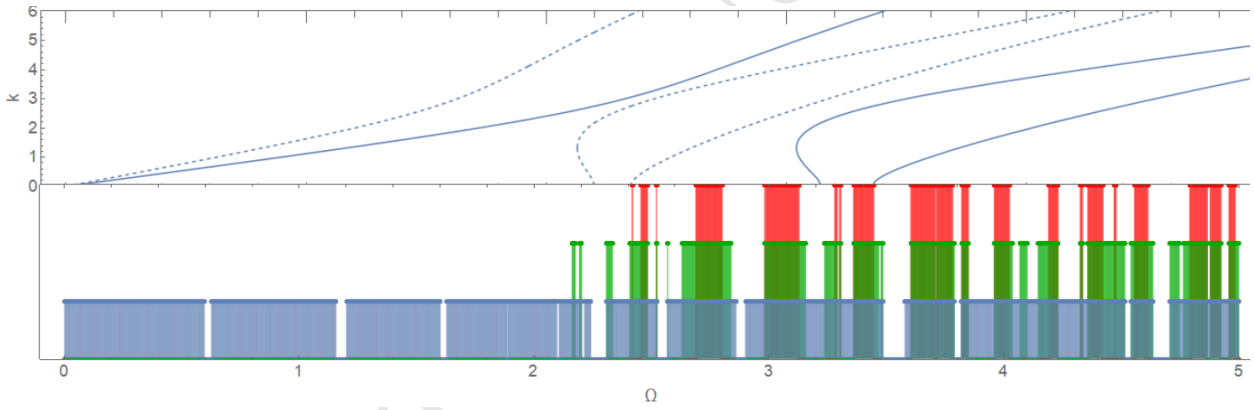

Figure 5: Upper: 3-mode theory dispersion diagrams (propagating waves only) "white" part –- solid, "black" part –- dashed; Lower –- Floquet modes first, second, third – from the bottom to the top, stop-bands –- blank, pass-bands –- color.

In Fig.5 upper part shows dispersion diagram for individually considered "white" and "grey" components for the 3-mode theory in frequency range from $\Omega = 0$ to $\Omega = 5$, where the second and the third Floquet modes begin to contribute to structural pass-bands. As seen, the cut-off frequencies of homogeneous 'white' and 'grey' components are, respectively, $\Omega_1^{white} = 3.04$, $\Omega_1^{grey} = 2.13$ and $\Omega_2^{white} = 3.35$, $\Omega_2^{grey} = 2.35$. Lower part of the Fig.5 shows the stop- and pass-bands of three Floquet modes. Colored zones represent partial pass-bands; white color is used to designate stop bands. One can see that, up to the frequency Ω_1^{grey}, pass-bands exist only for the first Floquet mode. As soon as more waves in a grey segment become propagating, the second and the third Floquet mode begin to contribute to pass-bands, despite that the white segment supports only one propagating wave until $\Omega_1^{white} = 3.04$. So, the frequencies Ω_1^{grey} and Ω_2^{grey} may be identified as the first and the second cut-off frequencies for Floquet modes in a periodic elastic layer.

Up to the first cut-off frequency, stop- and pass-band picture of a periodic structure is determined by a single Floquet mode, that is expressed with binomial $D_1^{(m)}$. Starting from

the first structural cut-off frequency up to the second, two Floquet modes are involved in formation of pass-bands, because two binomials $D_1^{(m)}$ and $D_2^{(m)}$ have separate stop- and pass-band picture.

Each polynomial has its own set of pass- and stop-bands and, therefore, one could distinguish between partial stop-bands, i.e. zones where only part of the active Floquet modes have stop-band, and full stop-bands for the periodic elastic layer. Difference between full and partial stop-bands is seen in Fig.5. At each structural cut-off frequency one more Floquet mode is activated in pass-band formation.

Although generation of partial pass-bands in a periodic multi-modal waveguide is similar to conventional transformation of evanescent waves to propagating ones in a homogeneous multi-modal waveguide at their cut-off frequencies, there are two major differences. First, in the latter case, a wave once converted to the propagating one remains propagating as frequency grows. Of course, the classical example of the opposite is the anomalous negative energy wave shown as the lower part of the second branch of dispersion diagram in Fig.2, but it converts back to propagating type as the third branch in the same diagram and does not undergo any further transformations. In a periodic structure, the Floquet mode is characterized by multiple intermittency of pass- and stop-bands after its cut-off. Second, each wave in a homogeneous layer is purely exponential (with a single uniquely defined either imaginary, or real, or complex argument, which continuously depends upon frequency following the dispersion relation), whereas each Floquet mode is composite, so that in each segment all free waves contributes to its formation. These observations will be elaborated further in discussion of comparison of the reduced-order models in Sec.5

Comparing the 1-mode Bernoulli model with the 3-mode model we conclude that, up to the first cut-off frequency of Floquet mode, the former one is qualitatively acceptable, because the waveguide properties of a periodic layer are determined by the single pair of propagation constants, which fulfills the condition $\Lambda^{(1)} * \Lambda^{(2)} = 1$.

The 5-mode theory is a natural expansion of 3-mode theory, and the modelling of a periodic layer by its means features the same properties, as modelling with 3-mode theory, see Fig.6. The diagram in Fig.6 is extended to frequencies, much higher than the upper frequency in Fig.5 in order to demonstrate contributions of the fourth and the fifth Floquet modes. We note that the frequency range, in which these modes contribute to formation of pass-bands, lies outside the range of validity of the 5-mode theory.

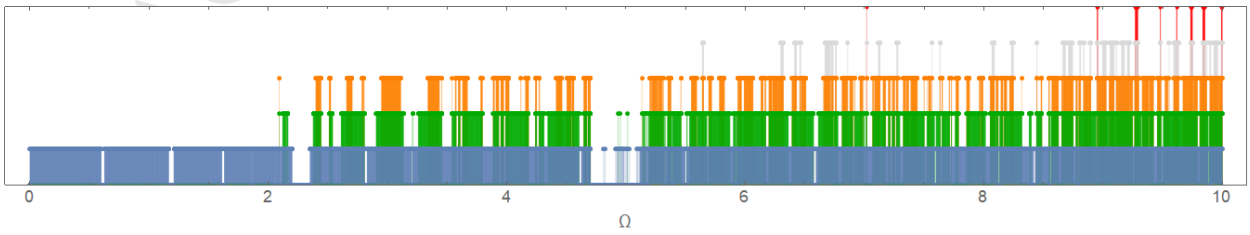

Figure 6: Pass- and stop-bands (color and blank respectively) for $D_1^{(5)}, ..., D_5^{(5)}$ (from the bottom to the top)

3.2. Energy flow analysis

To verify the predictions of the Floquet theory, we analyze energy flow in a semi-infinite elastic layer shown in Fig.7. It is loaded at the free end and variable number of periodicity cells with parameters specified by Eq.(2) are inserted. When the excitation frequency falls into the stop-bands, the insertion losses (IL) increase as the number of periodicity cells grows. In the pass-bands, IL is not sensitive to this number. The analysis is done in the framework of the 3-mode model.

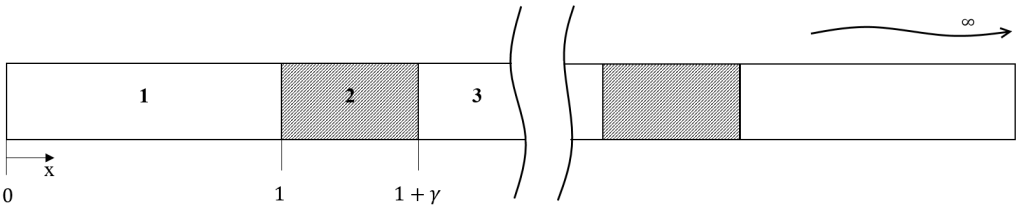

Figure 7: Energy flow scheme

Interfacial equations have the same form as Eq.(4), but for the last segment boundary equations are changed such that they satisfy Sommerfeld radiation conditions at infinity. Forcing conditions have the following form

$$\begin{aligned} F_0(0) &= 1 \\ U_1(0) &= 0 \\ F_2(0) &= 0 \end{aligned} \tag{11}$$

The energy flow for the structure with n periodic inclusions is found as (with vector definitions Eq.(3) and vector dot product $\cdot$)

$$E_n(x,\Omega) = \frac{1}{2}\Omega\,\mathrm{Re}[i(u^*(x)\cdot\sigma_{xx}(x) + v^*(x)\cdot\sigma_{xy}(x))] \tag{12}$$

With * in Eq.(12) complex conjugation is designated. We assume that E_0 is the energy flow through the semi-infinite layer without inclusions. We use the standard definition of IL

$$\mathrm{IL}(\Omega) = 10\log(\frac{E_0(\Omega)}{E_n(\Omega)}) \tag{13}$$

Energy in Eq.(12) can be found in any point within the layer due to the energy conservation property. Results of energy flow computation for the parameters Eq.(2) are shown in Fig.8. For illustrative matters, they are shown together with the stop-band picture, obtained for Eq.(7). Therefore, for illustrative matters insertion losses values are shown in this figure as $-1/10 * \mathrm{IL}(\Omega)$.

Energy flow analysis confirms, that in higher frequency region, where propagation is determined by more that one propagation constant, we can distinct the "full" stop-band, where all constants have property $\mathrm{abs}(\Lambda) \neq 1$ and "partial" stop-band where at least one constant has the property $\mathrm{abs}(\Lambda) = 1$, which is pass-band definition.

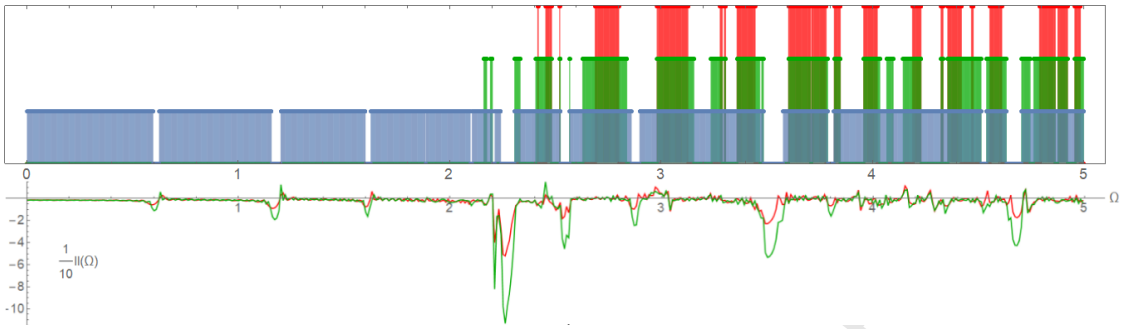

Figure 8: Energy flow for 20 (red) and 40 (green) periodic insertions versus the stop-band picture

4. The eigenfrequency problem for a finite layer

An infinite structure can be considered as an infinite sequence of finite periodic 'building blocks'. There is no unique choice of such a block, but, as shown in [10], the essential properties of an infinite periodic structure can be captured by means of the eigenfrequency analysis of a so-called unit symmetrical periodicity cell, shown on Fig.9.

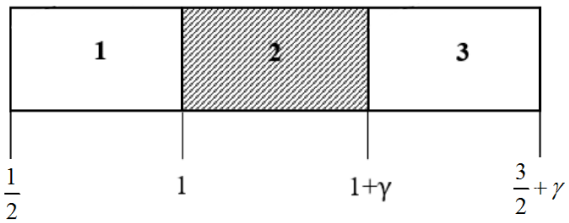

Figure 9: Symmetrical periodicity cell

Symmetrical boundary conditions should be posed in order to ensure that eigenfrequencies are located at the boundaries between stop- and pass-bands. In the case of the 1-mode Bernoulli-Euler model the choice is trivial: both ends can be either free or clamped.

The formulation of symmetrical boundary conditions, which ensure the same property of the eigenfrequency spectra, needs elaboration in more complicated cases, such as 3- 5-mode models. The bi-orthogonality relation uniquely defines these 'consistent' conditions. For the Rayleigh-Lamb problem, the bi-orthogonality relation has the following form [12]

$$\int_S (u^A \cdot \sigma^B_{xx} - v^B \cdot \sigma^A_{xy}) dS = 0 \tag{14}$$

It is a straightforward matter to demonstrate that, within the 5-mode model, this relation acquires the form

$$U^A_0(x)F^B_0(x) + U^A_2(x)F^B_2(x) + U^A_4(x)F^B_4(x) = V^B_1(x)F^A_1(x) + V^B_3(x)F^A_3(x) \tag{15}$$

The structure of bi-orthogonality relation (15) is fully explained in [8, Section 3.2]. For the 3-mode model, last terms in each side of equation Eq.(15) should be omitted, and for 1-mode Bernoulli-Euler model the bi-orthogonality relation does not exist.

In the case in hand, the kinematic and force state variable are divided into Class A and Class B functions as follows:

$$\begin{aligned}\mathbf{A}^{(i)}(x) &= \{\mathbf{u}_i(x), \sigma_{xx}^{(i)}(x)\} = \{U_0(x), U_2(x), U_4(x), F_1(x), F_3(x)\};\\ \mathbf{B}^{(i)}(x) &= \{\mathbf{v}_i(x), \sigma_{xy}^{(i)}(x)\} = \{V_1(x), V_3(x), F_0(x), F_2(x), F_4(x)\};\end{aligned} \tag{16}$$

Two sets of boundary conditions defined in a way, described above allows one to obtain eigenfrequencies placed on a stop-band boundary. Therefore, they can be called Class A and Class B boundary conditions. In explicit form, these conditions are written for a single symmetrical cell as

$$\begin{aligned}\mathbf{A}^{(1)}(1/2) &= 0\\ \mathbf{A}^{(3)}(3/2+\gamma) &= 0\end{aligned} \tag{17}$$

$$\begin{aligned}\mathbf{B}^{(1)}(1/2) &= 0\\ \mathbf{B}^{(3)}(3/2+\gamma) &= 0\end{aligned} \tag{18}$$

Interfacial conditions Eq.(4) and boundary conditions Eq.(17) and Eq.(18) define two systems of linear algebraic homogeneous equations to set up two eigenfrequency problems. Let $D_A(\Omega)$ and $D_B(\Omega)$ be the determinants of systems Eq.(4), Eq.(17) and Eq.(4), Eq.(18) respectively. Then eigenfrequencies can found from conditions $D_A^{(m)}(\Omega) = 0$ and $D_B^{(m)}(\Omega) = 0$.

In Fig.10 eigenfrequencies are schematically shown for a low frequency range, where only one Floquet mode is propagating

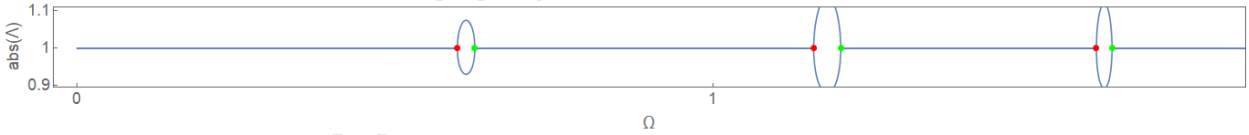

Figure 10: Eigenfrequencies of single symmetrical cell, 3-mode approximation A-type boundary conditions Eq.(17)(red) and B-type boundary conditions Eq.(18)(green)

The equivalence between the Class A/B eigenfrequency problem and the problem of finding the frequencies separating stop- and pass-bands for the Bernoulli-Euler theory has been rigorously proved in [10]. The same relation has been found for the 3-mode and 5-mode models. It has the following generalized form ($m = 1, 3, 5$):

$$D_A^{(m)}(\Omega) * D_B^{(m)}(\Omega) = C * \mathrm{discr}(D^{(m)}(\Lambda, \Omega)) = C * \prod_{j=1}^{m} \mathrm{discr}(D_j^{(m)}(\Lambda, \Omega)) \tag{19}$$

Since the polynomial $D^{(m)}(\Lambda, \Omega)$ in Λ for $m = 3$ and $m = 5$ has far more complicated form than one considered in [10], it is easier to find C numerically for each set of dimensionless parameters Eq.(1), rather than in the symbolic form.

For any set of these parameters, the product of eigenfrequency equations $D_A(\Omega) * D_B(\Omega)$ and the discriminant $\mathrm{discr}(D^{(m)}(\Lambda, \Omega))$ give transcendental equations of different form in Ω which, however, have only common roots.

Two transcendental equations have same set of roots if and only if they differ on a function, which does not have zeroes. Thus, unlike algebraic polynomial case, C contains function of Ω. As shown in [10], equations similar to the Eq.(9) and Eq.(19) for the case of axial rod vibration equation have the multipliers in form $a * \Omega^b$, where a is the complex constant and b - real-valued power. These multipliers are hardly recovered from a numerical solution. However, the coefficient, introduced in Eq.(19) can be recovered in the same form $C = a * \Omega^b$ from the fraction $C = \frac{\mathrm{discr}(D^{(m)}(\Lambda,\Omega))}{D_A^{(m)}(\Omega) * D_B^{(m)}(\Omega)}$ (it follows from Eq.(19)). For parameters set Eq.(2), we can numerically estimate the constant as $C = \frac{1}{5}\Omega^{\frac{205}{4}}$.

As follows from Eq.(19), eigenfrequencies of a single symmetrical periodicity cell are located on all partial stop-band boundaries. Therefore, the product $D_A(\Omega) * D_B(\Omega)$ has the sub-parts, that define eigenfrequencies placed on stop-band boundaries of each Floquet mode. In simple words, it means that each Floquet mode supports its own set of eigenfrequencies. However, mathematically rigorous proof of this fact is difficult even for relatively simple 3-mode theory and even if modern symbolic manipulators tools are used to execute algebraic manipulations in the general form. Therefore the series of numerical experiments have been conducted for validation.

We define partial eigenfrequencies equations as

$$D_A^{(m,j)}(\Omega) * D_B^{(m,j)}(\Omega) = C * \mathrm{discr}(D_j^{(m)}(\Lambda, \Omega)) \tag{20}$$

At the other hand product of partial eigenfrequency equations should give full eigenfrequency equation

$$D_A(\Omega) * D_B(\Omega) = \prod_{j=1}^{m} D_A^{(j)}(\Omega) * \prod_{j=1}^{m} D_B^{(j)}(\Omega) \tag{21}$$

Combining Eqs.(19-21) gives the equation, that can be used for direct computation

$$\begin{aligned} D_A^{(m,k)}(\Omega) &= \frac{D_A(\Omega)}{\sqrt{\prod\limits_{j\neq k} \mathrm{discr}(D_j^{(m)}(\Lambda,\Omega))}} \\ D_B^{(m,k)}(\Omega) &= \frac{D_B(\Omega)}{\sqrt{\prod\limits_{j\neq k} \mathrm{discr}(D_j^{(m)}(\Lambda,\Omega))}} \end{aligned} \tag{22}$$

Eigenfrequencies found from relation $D_A^{(m,1)}(\Omega) = 0$ and $D_B^{(m,1)}(\Omega) = 0$ match only stop-band boundaries of $D_1^{(m)}(\Lambda, \Omega)$, whereas Floquet zones of $D_q^{(m)}(\Lambda, \Omega)$, $q > 1$ remain unmarked.

In Fig.11, contributions of two Floquet modes to the eigenfrequency spectra for Class A and Class B boundary conditions are shown.

As seen from equation Eq.(19), there is a deep intrinsic link between the waveguide properties of an infinite periodic layer and the eigenfrequencies of a symmetric periodicity cell with Class A and Class B boundary conditions.

Here, we have, in the course of computations, found a much stronger relation Eq.(20), which features division of the eigenfrequency spectra into sub-spectra related to Floquet

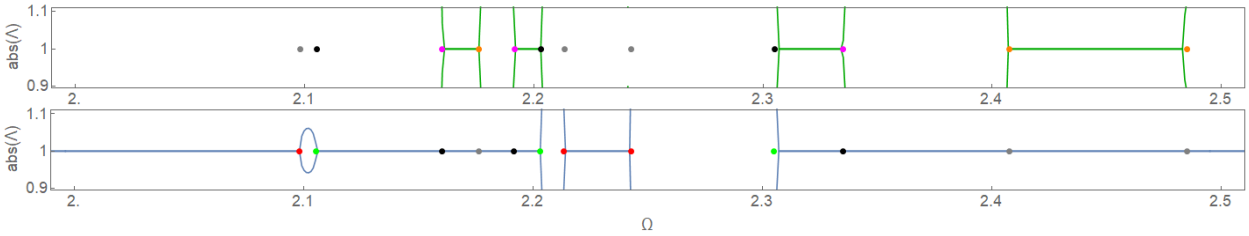

Figure 11: (lower part) Eigenfrequencies (mid-frequency range) defined by $D_A^{(1)}(\Omega)$ (red) and $D_B^{(1)}(\Omega)$ (green) and additional eigenfrequencies introduced by $D_A^{(2)}(\Omega)$ and $D_B^{(2)}(\Omega)$(grey and black respectively); (upper part) eigenfrequencies defined by $D_A^{(2)}(\Omega)$ (orange) and $D_B^{(2)}(\Omega)$(magenta) and eigenfrequencies introduced by $D_A^{(1)}(\Omega)$ and $D_B^{(1)}(\Omega)$ (grey and black respectively)

modes. The similar result is known in the theory of vibration of homogeneous Timoshenko beams as the so-called 'second eigenfrequency spectrum' debated in [13]. However, to the best of our knowledge, this factorization of eigenfrequency equations for a periodicity cell and of equations defining the borders between pass- and stop-bands for a periodic structure have not yet been documented in the literature. We note that we have obtained this results using the reduced-order modelling of wave propagation in a periodic elastic layer, and it would require much more computational efforts to spot it in the framework of the general formulation of the Rayleigh-Lamb problem. We also emphasize that the eigenfrequency problem for a symmetric periodicity cell with A- and B-type boundary conditions is a convenient tool to identify location of pass- and stop-bands in multi-modal periodic waveguides.

The eigenfrequency analysis of a finite structure, which consists of several symmetric cells has also been performed using the 3-mode and 5-mode models. The result presented in [10] for the Bernoulli-Euler 1-mode model has been fully confirmed: for Class A and Class B boundary conditions, eigenfrequencies of such a periodic structure are located in pass-bands. For these structures, regardless the number of periodicity cells, the set of eigenfrequencies located at the boundaries between pass- and stop-bands is found from the eigenfrequency analysis of the single periodicity cell.

5. Comparison of the models

Dispersion diagrams shown on a Fig.2 demonstrate the frequency ranges of applicability of reduced-order models to describe waveguide properties of homogeneous elastic layers. In this Section, we address the accuracy of these models in predictions of location of pass- and stop-bands in a periodic layer, taking full advantage of the equivalence between eigenfrequency and stop-bands problems and also of factorization of eigenfrequency spectra into Floquet modes.

Fig.12 illustrates the pass- and stop-bands of the first Floquet mode as predicted by 1-mode (Bernoulli-Euler), 3- and 5-mode theories. The pass-bands are shown as the horizontal strips of different colors, the stop bands, as in previous figures, are designated as white inserts. The first stop-band of this mode is predicted fairy well already by 1-mode theory.

However, there is the mismatch in location of the second stop-bands predicted by 1-mode and higher order theories. The 1-mode theory fails to predict the location of third stop band, while the agreement between the 3- and the 5-mode models remains satisfactory. There is a poor agreement in prediction of the location of the higher order stop-bands.

These three stop-bands are located in the frequency range, where only one Floquet mode contributes to the formation of pass-bands and only one wave propagates in each segment. As seen in Fig.2-Fig.3, there is a very reasonable agreement between the three theories in modelling of this wave in a homogeneous layer. Therefore, the result presented in Fig.12 may seem unexpected.

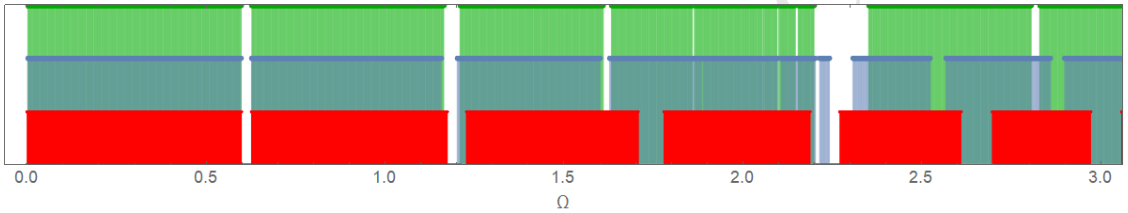

Figure 12: Pass-bands of a first Floquet mode predicted by approximation theories (from the bottom to the top) 1-mode , 3-mode, 5-mode

In order to explain this result, it is helpful to address first the eigenfrequency problem for a homogeneous segment with the same length as the periodicity cell. In Tab.1, the eigenfrequencies are presented both for all-white and all-grey segments. It should be noted that there is no difference between eigenfrequency spectra of homogeneous structures with Class A and Class B boundary conditions (when the trivial eigenfrequency corresponding to rigid body motion is excluded). Inspection into the shape of eigenmodes obtained in the framework of 3- and 5-mode models reveals that these eigenmodes are composed only as the superposition of the single pair of travelling waves characterized by the first branch of dispersion diagram shown in Fig.3 with no involvement of higher order modes. In effect, the difference between eigenfrequencies presented in Tab.1 is determined by the difference in wavenumbers predicted by the alternative theories (see Fig.2-Fig.3). The second eigenfrequency predicted by 1-mode model for white segment differs in 1.2% from its counterpart obtained with the 5-mode model. For a grey segment, the difference between the same eigenfequencies is 1.7%.

The eigenfrequencies of symmetric periodicity cell with Class A and Class B boundary conditions are summarized in Tab.2. These eigenfrequencies exactly match the borders of stop-bands shown in Fig.12, and, as already mentioned, the mismatch between the 1-mode theory and its 3- and 5-modes counterparts dramatically increases as frequency grows.

To explain the difference between accuracy levels of the elementary Bernoulli-Euler model in prediction of the eigenfrequencies of homogeneous and composite structures of the same length and with the same boundary conditions, it is necessary to inspect the shape of eigenmodes obtained in the framework of 1-, 3- and 5-mode models. In contrast to the case of a homogeneous periodicity cell, these eigenmodes for an inhomogeneous periodicity cell are composed as the superposition of all waves existing in its segments. The reason is that

Table 1: Eigenfrequencies of a finite homogenous layer, $L = 1 + \gamma = 11$

Approximation	Eigenfrequencies						
				1st cut-off			
1-mode	White	0.854233	1.67445				
3-mode		0.852385	1.64462	3.05498	3.08527	3.57845	3.97339
5-mode		0.853787	1.65539	2.95193	3.00065	3.60749	4.0027
1-mode	Grey	0.597963	1.17211				
3-mode		0.596669	1.15124	2.13848	2.15969	2.50491	2.78138
5-mode		0.597651	1.15877	2.06635	2.10046	2.52524	2.80189

Table 2: Eigenfrequencies of a symmetric periodicity cell

Approximation	1st stop-band		2nd stop-band		3rd stop-band	
	A-type	B-type	A-type	B-type	A-type	B-type
1-mode	0.598149	0.626777	1.17351	1.22713	1.70736	1.77976
3-mode	0.597367	0.625043	1.15773	1.20017	1.60196	1.62654
5-mode	0.59826	0.626175	1.16475	1.20875	1.6104	1.63175

the interfacial conditions between white and grey segments trigger the mode conversion.

Table 3: "Physical" amplitudes, 3-mode approximation

Amplitude/ Eigenfrequency		0.597367	0.625043	1.15773	1.20017	1.60196	1.62654
Wave 1	White	1	1	1	1	1	1
Wave 2		0	0.0032	0.0058	0.0205	0.0286	0.082
Wave 3		0	0	0.0017	0.006	0.009	0.03
Wave 1	Grey	0.70685	0.997	0.73	0.987	0.749	0.936
Wave 2		0.0008	0.00241	0.00914	0.01381	0.0525	0.049
Wave 3		0	0	0	0	0.00001	0.00002

As seen from Tab.3, the 'contamination' of the first wave in each segment by its higher-order counterparts (although evanescent in the frequency range in consideration) strongly affects the eigenfrequencies of a periodicity cell and, therefore, makes the mismatch of stop-band location visible.

The difference between 3-mode and 5-mode predictions is characterized in a different way in Fig.13 for the frequency $\Omega = 1.62654$ (3-mode) and $\Omega = 1.63175$ (5-mode), i.e., at the right boundary of the third stop-band, see last column in Table 2. Components of the standing wave in the 5-mode approximation are shown as solid lines, with dashed lines show the 3-mode approximation.

The Tab.4 presents relative amplitudes of each component of axial displacement in Legendre polynomial decomposition Eq.(3) for 5-mode theory. The numbers in each row are the ratios of these individual amplitudes to the total amplitude of the axial displacement,

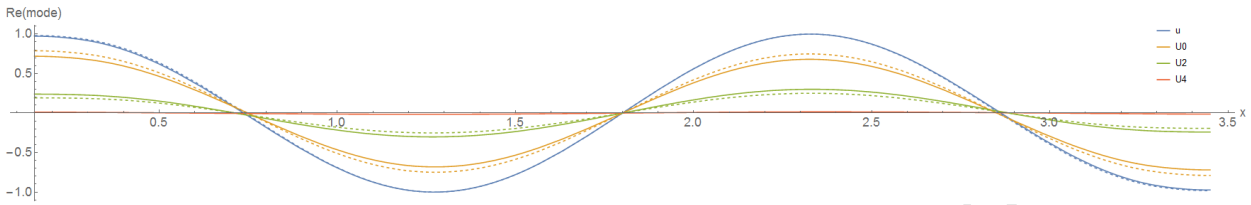

Figure 13: Eigenmode analysis, third stop-band, B-type boundary conditions

which is the sum of all modes in decomposition. Naturally, these amplitudes are determined as amplitudes of free waves multiplied with the appropriate modal coefficients and Tab.4 (if presented for the 3-mode model) would just re-scale the data from Tab.3. However, Tab.4 clearly demonstrates the significance of the component U_4 (ignored in the 3-mode theory) in formation of standing waves at the borders of the stop-bands. It explains the mismatch between 3-mode and 5-mode models in location of high-order stop-bands.

Table 4: Legendre polynomial decomposition amplitudes ratio

Mode	1st stop-band		2nd stop-band		3rd stop band	
	A-type	B-type	A-type	B-type	A-type	B-type
U0 ratio	0.983	0.981	0.908	0.896	0.717	0.686
U2 ratio	0.017	0.019	0.089	0.1	0.269	0.297
U4 ratio	0.0001	0.00006	0.003	0.003	0.012	0.015

Tab.4 shows that participation of mode U_4 in formation of the eigenmodes at the boundaries of the third stop-band is fairly small. It does not imply, however, validity of the 5-mode theory in the whole frequency range displayed in Fig.12. To estimate the frequency up to which the 5-mode theory is applicable, a more advanced model should be used. This task is out of the scope of this paper.

As seen from Tab.2-Tab.4, all waves, supported in infinite homogeneous 'grey' and 'white' layers are activated in a periodicity cell due to the mode conversion at the interfaces between the constituents, despite the 'consistent' Class A/B boundary conditions. Therefore, high accuracy of a given reduced order model in describing propagating waves in a homogeneous layer does not entail its equally high accuracy in identification of location of pass- and stop-bands in a periodic one.

6. Conclusions

The reported results suggest that the hierarchy of reduced-order models formulated in [8, 9] may be used for analysis of wave propagation in periodic elastic layers beyond the frequency range, where the elementary Bernoulli-Euler model is valid. These models allow identification of Floquet modes, and their simplicity (in comparison with approximate solutions of the original Rayleigh-Lamb problem) facilitates detailed studies of wave propagation in a periodic layer. By these means, we have made the following advances, each of which contains the aspect of novelty:

- We have demonstrated that properties of each Floquet mode may be analyzed individually. Therefore, it is plausible to deal with partial stop-bands, which need to overlap each other to create the full stop band. Similarly to any homogeneous waveguide, only one (the first) Floquet mode generates the low-frequency pass-band. The second Floquet mode is activated to produce pass-bands as soon as the frequency exceeds the first cut-off frequency of any single constituent of a periodic layer. Starting from this frequency, the elementary Bernoulli-Euler model becomes invalid.

- Within each member of the hierarchy of reduced-order models, the Class A and Class B boundary conditions are uniquely defined by the structure of the bi-orthogonality relations. The eigenfrequency spectra of symmetric unit periodicity cells with these boundary conditions coincide with the sets of frequencies separating the pass- and stop-bands of each Floquet mode in an infinite periodic elastic layer. Moreover, it is demonstrated that the eigenfrequency equations are factorized into subsets, each of which captures boundaries between partial pass- and stop-bands. This result generalizes the observations on the properties of eigenfrequencies of a single symmetrical cell or multi-modal periodic structure with its constituents modeled within Bernoulli-Euler beam or rod theories, Timoshenko beam theory and the theory of thin elastic cylindrical shells [10].

- We have demonstrated that the validity range of a given reduced order model for a periodic elastic layer is narrower, than its validity for a homogeneous one. The analysis of composition of eigenmodes of symmetric periodicity cells with Class A/B boundary conditions (standing waves at the boundaries between pass- and stop-bands) explains this effect. The interfacial conditions between components of a periodicity cell trigger mode conversion, so that all modes existing in each component are involved in the formation of a standing wave. Therefore, for example, as soon as contributions of the fourth and the fifth mode within 5- (or any higher-order) mode theory become significant, the 3-mode model ceases to be accurate. Similar statements are valid for higher order models.

As a final remark, we note that the computational efforts grow dramatically with the complexity of the model. It would have been much more difficult, if not at all possible to extract similar results from the numerical solution of the original Rayleigh-Lamb problem for a periodic elastic layer.

Appendix A. Hierarchy of reduced-order model governing equations

Modes are introduced with Legendre polynomial displacements decomposition, which can be written as

$$\begin{aligned} u(x,y,t) &= \sum_{i=0}^{m-2} \bar{U}_{2i}(x,t) * L_{2i}(y) \\ v(x,y,t) &= \sum_{i=1}^{m-2} \bar{V}_{2i-1}(x,t) * L_{2i-1}(y) \end{aligned} \tag{A.1}$$

,where $L_j(y)$ is the L^2-normalized Legendre polynomial of order j.

The governing equations are derived with the standard formulation of the action integral $H = \int\limits_S \int\limits_{t_1}^{t_2} [T - V] dt dS$ with definition of kinetic and elastic potential energy specific for the elastic layer

$$\begin{aligned} T &= \tfrac{1}{2}\rho \int\limits_S [(\tfrac{\partial u}{\partial t})^2 + (\tfrac{\partial v}{\partial t})^2] dS \\ V &= \tfrac{1}{2}\rho c_2^2 \int\limits_S [\sigma_{xx}\epsilon_{xx} + \sigma_{xy}\epsilon_{xy} + \sigma_{yy}\epsilon_{yy}] dS \end{aligned} \tag{A.2}$$

The Hamilton's principle $\delta H = 0$ is used with Eq.(A.1) for $m = 1, 3, 5$ substituted in Eq.(A.2). By these means, the following eqations are obtained:

a) Bernoulli-Euler single-mode theory

$$-\frac{\partial^2 \bar{U}_0(x,t)}{\partial t^2} + \frac{4(\eta^2 - 1)}{\eta^2} c_2^2 \frac{\partial^2 \bar{U}_0(x,t)}{\partial x^2} = 0 \tag{A.3}$$

The boundary conditions at the edges of an elastic layer $x = a$, $x = b$ are concerned with

$$\bar{U}_0(x,t) \text{ or } \bar{F}_0(x,t) \equiv -\frac{4(\eta^2 - 1)}{\eta^2} \frac{\partial \bar{U}_0(x,t)}{\partial x} \tag{A.4}$$

b) The three-mode theory

$$\begin{gathered} \eta^2 \tfrac{\partial^2 \bar{U}_0(x,t)}{\partial x^2} - \tfrac{1}{c_2^2} \tfrac{\partial^2 \bar{U}_0(x,t)}{\partial t^2} - (2 - \eta^2) \tfrac{\partial \bar{V}_1(x,t)}{\partial x} = 0 \\ (2 - \eta^2) \tfrac{\partial \bar{U}_0 x,t}{\partial x} + \tfrac{1}{12} \tfrac{\partial^2 \bar{V}_1(x,t)}{\partial x^2} - \eta^2 V_1(x,t) - \tfrac{1}{\pi^2} \tfrac{1}{c_2^2} \tfrac{\partial^2 \bar{V}_1(x,t)}{\partial t^2} - 2 \tfrac{\partial \bar{U}_2(x,t)}{\partial x} = 0 \\ 2 \tfrac{\partial \bar{V}_1(x,t)}{\partial x} + \tfrac{4}{5} \eta^2 \tfrac{\partial^2 \bar{U}_2(x,t)}{\partial x^2} - 48 \bar{U}_2(x,t) - \tfrac{12}{\pi^2} \tfrac{1}{c_2^2} \tfrac{\partial^2 \bar{U}_2(x,t)}{\partial t^2} = 0 \end{gathered} \tag{A.5}$$

The boundary conditions at the edges $x = a$, $x = b$ are concerned with the following pairs of generalized forces and displacements:

$$\begin{gathered} \bar{F}_0(x,t) \equiv \eta^2 \tfrac{\partial \bar{U}_0(x,t)}{\partial x} + (\eta^2 - 2)\, \bar{V}_1(x,t) \text{ and } \bar{U}_0(x,t) \\ \bar{F}_1(x,t) \equiv \tfrac{1}{12} \tfrac{\partial \bar{V}_1(x,t)}{\partial x} - 2 \bar{U}_2(x,t) \text{ and } \bar{V}_1(x,t) \\ \bar{F}_2(x,t) \equiv \tfrac{4}{5} \eta^2 \tfrac{\partial \bar{U}_2(x,t)}{\partial x} \text{ and } \bar{U}_2(x,t) \end{gathered} \tag{A.6}$$

c) The five-mode theory

$$\begin{gathered} \eta^2 \tfrac{\partial^2 \bar{U}_0(x,t)}{\partial x^2} - \tfrac{1}{c_2^2} \tfrac{\partial^2 \bar{U}_0(x,t)}{\partial t^2} - (2 - \eta^2)\, \tfrac{\partial \bar{V}_1(x,t)}{\partial x} + 2\sqrt{7}\, (2 - \eta^2)\, \tfrac{\partial \bar{V}_3(x,t)}{\partial x} = 0 \\ (2 - \eta^2)\, \tfrac{\partial \bar{U}_0(x,t)}{\partial x} + \tfrac{1}{12} \tfrac{\partial^2 \bar{V}_1(x,t)}{\partial x^2} - \eta^2 \bar{V}_1(x,t) - \tfrac{1}{12} \tfrac{1}{c_2^2} C_{21} \tfrac{\partial^2 \bar{V}_1(x,t)}{\partial t^2} - 2 \tfrac{\partial \bar{U}_2(x,t)}{\partial x} + \\ + 2\eta^2 \sqrt{7} \bar{V}_3(x,t) + 3 \tfrac{\partial \bar{U}_4(x,t)}{\partial x} = 0 \\ 2 \tfrac{\partial \bar{V}_1(x,t)}{\partial x} + \tfrac{4}{5} \eta^2 \tfrac{\partial^2 \bar{U}_2(x,t)}{\partial x^2} - 48 \bar{U}_2(x,t) - \tfrac{4}{5} \tfrac{1}{c_2^2} C_{22} \tfrac{\partial^2 \bar{U}_2(x,t)}{\partial t^2} - \\ - 4\sqrt{7}\, (2 - \eta^2)\, \tfrac{\partial \bar{V}_3(x,t)}{\partial x} + 72 \bar{U}_4(x,t) = 0 \\ -2\sqrt{7}\, (2 - \eta^2)\, \tfrac{\partial \bar{U}_0(x,t)}{\partial x} + 2\alpha^2 \sqrt{7} \bar{V}_1(x,t) + 4\sqrt{7}\, (2 - \eta^2)\, \tfrac{\partial \bar{U}_2(x,t)}{\partial x} + \tfrac{\partial^2 \bar{V}_3(x,t)}{\partial x^2} - \\ - 168 \eta^2 \bar{V}_3(x,t) - \tfrac{1}{c_2^2} C_{23} \tfrac{\partial^2 \bar{V}_3(x,t)}{\partial t^2} - 6\sqrt{7} \tfrac{\partial \bar{U}_4(x,t)}{\partial x} = 0 \end{gathered} \tag{A.7}$$

The inertia correction factors are:

$$C_{21} = \frac{2\left(25+\sqrt{355}\right)}{9\pi^2}, C_{22} = \frac{3\left(35+\sqrt{105}\right)}{16\pi^2}, C_{23} = \frac{56\left(25-\sqrt{355}\right)}{9\pi^2}, C_{24} = \frac{9\left(35-\sqrt{105}\right)}{4\pi^2} \tag{A.8}$$

The boundary conditions are concerned with the following pairs of generalised forces and displacements:

$$\begin{gathered}
\bar{F}_0(x,t) \equiv \eta^2 \tfrac{\partial \bar{U}_0(x,t)}{\partial x} + \left(\eta^2-2\right)\bar{V}_1(x,t) - 2\sqrt{7}\left(\eta^2-2\right)\bar{V}_3(x,t) \text{ and } \bar{U}_0(x,t) \\
\bar{F}_1(x,t) \equiv \tfrac{1}{12}\tfrac{\partial \bar{V}_1(x,t)}{\partial x} - 2\bar{U}_2(x,t) + 3\bar{U}_4(x,t) \text{ and } \bar{V}_1(x,t) \\
\bar{F}_2(x,t) \equiv \tfrac{4}{5}\eta^2 \tfrac{\partial \bar{U}_2(x,t)}{\partial x} + 4\sqrt{7}\left(\eta^2-2\right)\bar{V}_3(x,t) \text{ and } \bar{U}_2(x,t) \\
\bar{F}_3(x,t) \equiv \tfrac{\partial \bar{V}_3(x,t)}{\partial x} - 6\sqrt{7}\bar{U}_4(x,t) \text{ and } \bar{V}_3(x,t) \\
\bar{F}_4(x,t) \equiv \eta^2 \tfrac{\partial \bar{U}_4(x,t)}{\partial x} \text{ and } \bar{U}_4(x,t)
\end{gathered} \tag{A.9}$$

After governing equations are obtained, modes are substituted with dependence of all state variables taken as $\exp(-i\omega t)$, i.e. $\bar{U}_0(x,t) = U_0(x)\exp(-i\omega t)$ (other projection modes are defined analogously).

With spatial dependency $\exp(ikx)$ following form for every projection is obtained (for brievity only U_0 mode is shown)

$$\bar{U}_0(x,t) = U_0 \exp(ikx - i\omega t) \tag{A.10}$$

Modes in form Eq.(A.10) are substituted in Eq.(A.3) for 1-mode theory, in Eq.(A.5) for 3-mode theory and in Eq.(A.7) for 5-mode theory After cancellation of the dependency term $\exp(ikx-i\omega t)$ one obtain homogeneous system of m equations with respect to unknown amplitudes U_p,V_q. Determinant of this system contains k and Ω as parameters and define dispersion relation $k_m(\Omega)$ in the polynomial form.

References

[1] L.Brillouin, Wave Propagation in Periodic Structures second ed., Dover Publications New York, 1953.

[2] D. Mead, Wave propagation in continuous periodic structures: Research contributions from southampton, 1964–1995, Journal of Sound and Vibration 190 (3) (1996) 495 – 524. doi:https://doi.org/10.1006/jsvi.1996.0076.
URL http://www.sciencedirect.com/science/article/pii/S0022460X96900760

[3] D. Mead, Wave propagation and natural modes in periodic systems: I. mono-coupled systems, Journal of Sound and Vibration 40 (1) (1975) 1 – 18. doi:https://doi.org/10.1016/S0022-460X(75)80227-6.
URL http://www.sciencedirect.com/science/article/pii/S0022460X75802276

[4] D. Mead, Wave propagation and natural modes in periodic systems: Ii. multi-coupled systems, with and without damping, Journal of Sound and Vibration 40 (1) (1975) 19 – 39. doi:https://doi.org/10.1016/S0022-460X(75)80228-8.
URL http://www.sciencedirect.com/science/article/pii/S0022460X75802288

[5] S. D. Adams, R. V. Craster, S. Guenneau, Bloch waves in periodic multi-layered acoustic waveguides, Proceedings of the Royal Society of London A: Mathematical, Physical and Engineering Sciences 464 (2098) (2008) 2669–2692. arXiv:http://rspa.royalsocietypublishing.org/content/

464/2098/2669.full.pdf, doi:10.1098/rspa.2008.0065.
URL http://rspa.royalsocietypublishing.org/content/464/2098/2669

[6] R. V. Craster, J. Kaplunov, A. V. Pichugin, High-frequency homogenization for periodic media, Proceedings of the Royal Society of London A: Mathematical, Physical and Engineering Sciences 466 (2120) (2010) 2341–2362. arXiv:http://rspa.royalsocietypublishing.org/content/466/2120/2341.full.pdf, doi:10.1098/rspa.2009.0612.
URL http://rspa.royalsocietypublishing.org/content/466/2120/2341

[7] V. Pagneux, A. Maurel, Lamb wave propagation in inhomogeneous elastic waveguides, Proceedings: Mathematical, Physical and Engineering Sciences 458 (2024) (2002) 1913–1930.
URL http://www.jstor.org/stable/3067190

[8] S. Sorokin, C. Chapman, A hierarchy of high-order theories for symmetric modes in an elastic layer, Journal of Sound and Vibration 333 (15) (2014) 3505 – 3521. doi:https://doi.org/10.1016/j.jsv.2014.03.005.
URL http://www.sciencedirect.com/science/article/pii/S0022460X14001850

[9] S. Sorokin, R. Kolman, J. Kopacka, The boundary integral equations method for analysis of high-frequency vibrations of an elastic layer, Archive of Applied Mechanics 87 (4) (2017) 737–750. doi:10.1007/s00419-016-1220-y.
URL https://doi.org/10.1007/s00419-016-1220-y

[10] A. Hvatov, S. Sorokin, Free vibrations of finite periodic structures in pass- and stop-bands of the counterpart infinite waveguides, Journal of Sound and Vibration 347 (2015) 200 – 217. doi:https://doi.org/10.1016/j.jsv.2015.03.003.
URL http://www.sciencedirect.com/science/article/pii/S0022460X15002217

[11] A. Soe-Knudsen, On advantages of derivation of exact dynamical stiffness matrices from boundary integral equations, The Journal of the Acoustical Society of America 128 (2) (2010) 551–554. arXiv:https://doi.org/10.1121/1.3455794, doi:10.1121/1.3455794.
URL https://doi.org/10.1121/1.3455794

[12] W. B. Fraser, Orthogonality relation for the rayleigh–lamb modes of vibration of a plate, The Journal of the Acoustical Society of America 59 (1) (1976) 215–216. arXiv:https://doi.org/10.1121/1.380851, doi:10.1121/1.380851.
URL https://doi.org/10.1121/1.380851

[13] N. Stephen, The second spectrum of timoshenko beam theory—further assessment, Journal of Sound and Vibration 292 (1) (2006) 372 – 389. doi:https://doi.org/10.1016/j.jsv.2005.08.003.
URL http://www.sciencedirect.com/science/article/pii/S0022460X05005213